

THE SINS/ZC-SINF SURVEY OF $z \sim 2$ GALAXY KINEMATICS: THE NATURE OF DISPERSION DOMINATED GALAXIES*

SARAH F. NEWMAN^{1,17}, REINHARD GENZEL^{1,2,3}, NATASCHA M. FÖRSTER SCHREIBER², KRISTEN SHAPIRO GRIFFIN⁴, CHIARA MANCINI⁵, SIMON J. LILLY⁶, ALVIO RENZINI⁵, NICOLAS BOUCHÉ^{7,8}, ANDREAS BURKERT⁹, PETER BUSCHKAMP², C. MARCELLA CAROLLO⁶, GIOVANNI CRESCI¹⁰, RIC DAVIES², FRANK EISENHAEUER², SHY GENEL¹¹, ERIN K. S. HICKS¹², JARON KURK², DIETER LUTZ², THORSTEN NAAB¹³, YINGJIE PENG⁶, AMIEL STERNBERG¹⁴, LINDA J. TACCONI², STIJN WUYTS², GIANNI ZAMORANI¹⁵, AND DANIELA VERGANI¹⁶

Draft version April 3, 2013

ABSTRACT

We analyze the spectra, spatial distributions and kinematics of $H\alpha$, [NII] and [SII] emission in a sample of 38, $z \sim 2.2$ UV/optically selected star forming galaxies (SFGs) from the SINS & zC-SINF surveys, 34 of which were observed in the adaptive optics mode of SINFONI and 30 of those contain data presented for the first time here. This is supplemented by kinematic data from 43 $z \sim 1-2.5$ galaxies from the literature. None of these 81 galaxies is an obvious major merger. We find that the kinematic classification of high- z SFGs as ‘dispersion dominated’ or ‘rotation dominated’ correlates most strongly with their intrinsic sizes. Smaller galaxies are more likely ‘dispersion-dominated’ for two main reasons: 1) The rotation velocity scales linearly with galaxy size but intrinsic velocity dispersion does not depend on size or may even increase in smaller galaxies, and as such, their ratio is systematically lower for smaller galaxies, and 2) Beam smearing strongly decreases large-scale velocity gradients and increases observed dispersion much more for galaxies with sizes at or below the resolution. Dispersion dominated SFGs may thus have intrinsic properties similar to ‘rotation dominated’ SFGs, but are primarily more compact, lower mass, less metal enriched and may have higher gas fractions, plausibly because they represent an earlier evolutionary state.

Subject headings: galaxies: high redshift – galaxies: evolution – infrared: galaxies

1. INTRODUCTION

* Based on observations at the Very Large Telescope (VLT) of the European Southern Observatory (ESO), Paranal, Chile (ESO program IDs 076.A-0527, 079.A-0341, 080.A-0330, 080.A-0339, 080.A-0635, 183.A-0781).

¹ Department of Astronomy, Campbell Hall, University of California, Berkeley, CA 94720, USA

² Max-Planck-Institut für extraterrestrische Physik (MPE), Giessenbachstr.1, D-85748 Garching, Germany

³ Department of Physics, Le Conte Hall, University of California, Berkeley, CA 94720, USA

⁴ Space Sciences Research Group, Northrop Grumman Aerospace Systems, Redondo Beach, CA 90278, USA

⁵ Osservatorio Astronomico di Padova, Vicolo dell’Osservatorio 5, Padova, I-35122, Italy

⁶ Institute of Astronomy, Department of Physics, Eidgenössische Technische Hochschule, ETH Zürich, CH-8093, Switzerland

⁷ Université de Toulouse; UPS-OMP; IRAP; Toulouse, France
⁸ CNRS; IRAP; 14, avenue Edouard Belin, F-31400 Toulouse, France

⁹ Universitäts-Sternwarte Ludwig-Maximilians-Universität (USM), Scheinerstr. 1, München, D-81679, Germany

¹⁰ Istituto Nazionale di Astrofisica Osservatorio Astronomico di Arcetri, Largo Enrico Fermi 5, I 50125 Firenze, Italy

¹¹ Harvard-Smithsonian Center for Astrophysics, 60 Garden Street, Cambridge, MA 02138 USA

¹² Department of Astronomy, University of Washington, Box 351580, U.W., Seattle, WA 98195-1580, USA

¹³ Max-Planck Institute for Astrophysics, Karl Schwarzschildstrasse 1, D-85748 Garching, Germany

¹⁴ School of Physics and Astronomy, Tel Aviv University, Tel Aviv 69978, Israel

¹⁵ INAF Osservatorio Astronomico di Bologna, Via Ranzani 1, 40127 Bologna, Italy

¹⁶ INAF Istituto di Astrofisica Spaziale e Fisica Cosmica di Bologna, Via P. Gobetti 101, 40129 Bologna, Italy

¹⁷ email: sfnewman@berkeley.edu

At the peak of the galactic formation epoch at $z \sim 1-3$, the rest-frame UV and $H\alpha$ morphologies of most star forming galaxies near the ‘main sequence’ of the stellar mass-star formation plane (henceforth ‘SFGs’: Noeske et al. 2007; Daddi et al. 2007; Rodighiero et al. 2011; Peng et al. 2010) are typically irregular and in some cases dominated by several giant (kpc-size) star forming clumps (Cowie et al. 1995; van den Bergh et al. 1996; Elmegreen et al. 2004, 2009; Elmegreen & Elmegreen 2005, 2006; Genzel et al. 2006, 2008, 2011; Law et al. 2007, 2009, 2012a; Förster Schreiber et al. 2009, 2011; Wuyts et al. 2012; Swinbank et al. 2012a,b). The ionized gas kinematics of these clumpy galaxies range from rotationally supported disks, especially among the more massive ($M_* \geq$ a few $10^{10} M_\odot$) and bright (Ks AB ≤ 21.8) SFGs, to galaxies dominated by apparently random motions (Förster Schreiber et al. 2006, 2009; Law et al. 2007, 2009; Genzel et al. 2008, 2011; Wright et al. 2007, 2009; Shapiro et al. 2008; Cresci et al. 2009; van Starkenburg et al. 2008; Epinat et al. 2009; Lemoine-Busserolle & Lamareille 2010; Jones et al. 2012; Wisnioski et al. 2012; Swinbank et al. 2012a,b; Epinat et al. 2012). The latter class, which are especially common among the smaller and lower mass systems, often have average intrinsic velocity dispersions (corrected for instrumental broadening and beam smearing, and determined here from the outer regions of the galaxies), σ_0 , larger than the inclination-corrected rotation velocities, v_{rot} (hereafter, ‘dispersion dominated’ SFGs) (Förster Schreiber et al. 2009). Despite these irregular morphologies, the fraction of major mergers is probably less than 30% (Shapiro et al. 2008; Förster Schreiber et al. 2009; López-Sanjuan et al. 2012) and stellar mass maps of $z \sim 1-2$ SFGs are typically

smoother and more symmetric than the light distributions (Wuyts et al. 2012). As a rule, rest-frame UV and optically-selected high- z SFGs exhibit large local random motions, with ratios of v_{rot} to σ_0 of less than 8. Hence even the rotationally dominated systems are thick ($H_z \sim 1$ kpc; Elmegreen & Elmegreen 2006) and highly turbulent. Observations of CO rotational line emission indicate that $z \sim 1-3$ massive SFGs have large ($\sim 30-60\%$) baryonic cold gas fractions and this cold molecular gas has a large velocity dispersion comparable to that of the warm ionized gas traced by $H\alpha$ (Daddi et al. 2008, 2010a; Tacconi et al. 2008, 2010, 2012; Swinbank et al. 2011).

These basic observational properties (irregular morphologies, high gas fractions and large velocity dispersions) can be understood in a simple physical framework, in which global gravitational instability and fragmentation in marginally stable ($Q_{Toomre} \leq 1$), gas-rich disks naturally leads to large turbulence and the formation of giant star forming clumps (Noguchi 1999; Immeli et al. 2004a,b; Bournaud et al. 2007; Elmegreen et al. 2008; Genzel et al. 2008, 2011; Dekel et al. 2009; Bournaud et al. 2010; Genel et al. 2012b). The buildup of these marginally stable disks in $z > 1$ SFGs is plausibly fueled mainly by smooth accretion of gas and/or minor mergers (Kereš et al. 2005, 2009; Dekel & Birnboim 2006; Bower et al. 2006; Kitzbichler & White 2007; Ocvirk et al. 2008; Davé 2008; Dekel et al. 2009; Oser et al. 2010; Cacciato et al. 2012; Ceverino et al. 2012).

While the buildup of early star forming disks may be explained by this scenario, it is less clear how the dispersion dominated galaxies fit in. There are several possible explanations for what they are (see e.g.: Förster Schreiber et al. 2009; Law et al. 2007, 2009, 2012a; Jones et al. 2010; Epinat et al. 2012), including:

- (1) an earlier evolutionary stage with higher gas fractions and lower masses, in which case the simple fragmentation scenario discussed above would lead to larger velocity dispersions,
- (2) intrinsically smaller rotationally supported disks that masquerade as dispersion dominated because the instrumental ‘beam smearing’ hides the rotational signal,
- (3) the result of dissipative major mergers that would drive chaotic motions,
- (4) giant clumps in face-on star forming disks, where the rest of the disk material has too low surface brightness to be detected, or
- (5) some combination thereof.

In this paper we present and analyze new high-quality SINFONI/VLT integral field (IFU) spectroscopy with natural and laser guide star adaptive optics (AO) (Eisenhauer et al. 2003; Bonnet et al. 2004) of 30 $z \sim 2$ SFGs. We combine this with 4 AO and 4 seeing-limited data sets which have been presented previously by our group (Förster Schreiber et al. 2009; Cresci et al. 2009; Genzel et al. 2011), but contain new analysis here. For these 38 SINS/zC-SINF galaxies, we find that 43% were classified as ‘dispersion dominated’ based on previous seeing limited observations and according to the criteria of Förster

Schreiber et al. (2009). We add to our measurements another 35 AO data sets and 8 spatially well-resolved (with $R_{1/2} > 4.5$ kpc) seeing limited data sets of $z = 1-2.5$ SFGs from the literature. The combined data of 81 SFGs provide interesting new constraints on the nature of the dispersion dominated SFG population. We adopt a Λ CDM cosmology with $\Omega_m = 0.27$, $\Omega_b = 0.046$ and $H_0 = 70$ km/s/Mpc (Komatsu et al. 2011), as well as a Chabrier (2003) initial stellar mass function (IMF).

2. OBSERVATIONS AND ANALYSIS

2.1. Source selection, observations and data reduction of SINS/zC-SINF galaxies

Our base sample are 34 SFGs from the SINS and zC-SINF surveys of $H\alpha + [NII]$ integral field spectroscopy in $z \sim 1.5-2.5$ SFGs obtained with SINFONI on the ESO VLT that were observed in both seeing-limited and AO mode. These galaxies are drawn from the parent seeing-limited SINFONI samples described in Förster Schreiber et al. (2009) and Mancini et al. (2011). The main criteria for selecting these galaxies from the seeing-limited sample were a clear detection of $H\alpha$ in one hour seeing-limited SINFONI data, the proximity of a suitably bright AO reference star, and the goal of ultimately covering as much of the range in stellar mass, SFR and kinematic properties of the parent no-AO SINS/zC-SINF sample as possible. The resulting AO sample has nearly identical distributions in M_* and SFR as the parent no-AO sample in terms of range, median and offset from the main sequence (Förster Schreiber et al. 2013). In addition to the SINS/zC-SINF AO sample, we include 4 large galaxies ($R_{1/2} > 4.5$ kpc) observed only in seeing-limited mode with sufficient signal to noise ratio (S/N) and spatial resolution to robustly determine the kinematics (Förster Schreiber et al. 2009; Mancini et al. 2011). Adding these larger objects does not bias our results as we do not aim for a ‘complete’ sample, merely one that has as large a range in galaxy properties and kinematic types as possible. Thus these galaxies only give us more information on rotationally-supported objects. We exclude obvious major mergers from our sample, but keep possible minor mergers, assuming that the central object in a minor merger retains its kinematic integrity to a significant extent. Note, however, that this criterion only eliminated 5 out of originally 86 objects (when including the additional datasets from the literature - see next Section).

The SINS and zC-SINF surveys were selected either from their U_n GR colors satisfying the ‘BX’ criteria (Steidel et al. 2004; Adelberger et al. 2004; Erb et al. 2006; Law et al. 2009) or based on K band imaging via the ‘BzK’ criterion for $1.4 < z < 2.5$ SFGs (Daddi et al. 2004b). In addition, a few galaxies were included based on their stellar masses and SFRs from the GMASS Spitzer $4\mu m$ survey (Kurk et al. 2009, 2013), and one galaxy was selected from the GDDS survey based on a secure redshift and evidence for on-going star-formation from the UV data (Abraham et al. 2004).

These galaxies sample the $z \sim 2$ SFG ‘main sequence’ in the stellar mass – star-formation rate plane between stellar masses of $10^{9.2}$ and $10^{11.5} M_\odot$, and star formation rates between ~ 13 and $850 M_\odot \text{yr}^{-1}$ (see Figure 1), covering the same range in M_* and SFR as the parent

samples. For the AO data, we employed SINFONI in the $0.05'' \times 0.1''$ pixel scale, with either laser guide star (LGS) or natural guide star (NGS) AO, resulting in angular resolutions of $\sim 0.20''$ (equivalent to 1.7 kpc at $z \sim 2$) full width at half maximum (FWHM) after median filtering by 3×3 pixels. The 4 larger rotationally supported systems were observed in SINFONI's seeing limited mode and $0.125'' \times 0.25''$ pixel scale, resulting in a median FWHM $\sim 0.56''$, sufficient to resolve these SFGs (Förster Schreiber et al. 2009). These sources are included in the analysis (and not other seeing-limited only galaxies), because their large spatial extents allow well-resolved kinematical analysis. The on-source integration times for each galaxy from our sample range between 2 and 23 hours, with a median of about 5.8 hours, resulting in high quality, spatially resolved spectra for most sources. This sample includes 6 AGN, identified by the presence of AGN signatures in their rest-UV spectrum, $[\text{NII}]/\text{H}\alpha$ ratio, and/or X-ray or MIPS $24\mu\text{m}$ data when available (e.g., see Förster Schreiber et al. 2009). These would not affect our σ_0 measurements, which are taken away from the center, but could potentially affect σ_{tot} (the total Gaussian line width integrated over the source). A discussion of the properties of 9 individual galaxies of the AO sample can be found in several of our earlier SINS papers (Genzel et al. 2006, 2011; Cresci et al. 2009; Förster Schreiber et al. 2009; Newman et al. 2012a), with new data here for 5 of those objects. A detailed discussion of the full AO sample will be presented in Förster Schreiber et al. (2013).

We used the software package SPRED and custom routines for optimizing the background/OH airglow subtraction for the data reduction. The point spread function (PSF) FWHM was measured by fitting a 2D Gaussian profile to the combined images of the PSF calibration star taken throughout the observations of a galaxy. More information on the specifics of these observations and the data reduction can be found in Förster Schreiber et al. (2009); Mancini et al. (2011); Förster Schreiber et al. (2013).

We created $\text{H}\alpha$ emission line, velocity and velocity dispersion maps from the reduced data cubes by using the Gaussian-fitting procedure LINEFIT (Davies et al. 2011), with errors derived from the noise cube. For more information on our standard SINS data reduction methods and analysis tools we refer to Schreiber et al. (2004); Davies (2007); Förster Schreiber et al. (2009); Mancini et al. (2011).

2.2. Additional datasets from the literature

We also include in our analysis 43 additional $z \sim 1-2.5$ SFGs from the literature (Table 1) deriving from IFU datasets with beam-smearing corrected kinematic information. These include:

- 9 galaxies from the BX- (rest-UV color/magnitude) selected $z = 1.5-2.5$ AO sample from Law et al. (2009, 2012c) taken with OSIRIS.
- 6 galaxies from the BM-selected $z = 1.5-1.7$ AO sample from Wright et al. (2007, 2009) taken with OSIRIS.
- 12 galaxies from the $z = 1.3-1.45$ AO sample from Wisnioski et al. (2011) selected for strong [OII]

emission from the Wiggle-Z Dark Energy (UV-selected) survey, also taken with OSIRIS.

- 5 $z \sim 1.45$ galaxies from Swinbank et al. (2012a,b), taken from the HiZELS imaging survey of the COSMOS and UDS fields, selected for narrow band $\text{H}\alpha$ flux and observed with SINFONI in the AO mode.
- 8 $z = 1-1.6$ MASSIV galaxies selected from the VVDS spectroscopic survey observed in seeing-limited mode with SINFONI (Lemoine-Busserolle & Lamareille 2010; Epinat et al. 2012; Contini et al. 2012; Vergani et al. 2012). Here we only chose galaxies with $R_{1/2} > 4.5$ kpc, such that their kinematics could be well resolved without AO.
- 3 additional $z = 1.2-1.4$ galaxies from Epinat et al. (2012) observed in the AO mode of SINFONI.

These galaxies were selected such that they were in the redshift interval 1–2.5, were not classified as major mergers, and had either AO data or seeing-limited data with $R_{1/2} > 4.5$ kpc. We do not include $z < 1$ studies (Puech et al. 2007, 2009; Neichel et al. 2008, e.g.), or $z \sim 1$ slit spectroscopy (Weiner et al. 2006; Kassin et al. 2007) in the analysis, but emphasize that these investigations also find evidence for large random motions.

Figure 1 shows the location of our entire sample in the SFR- M_* plane. As can be seen from the left panel, SFGs are well-sampled from a SFR of 10 to 500 M_\odot/yr and over 2 decades of stellar mass, from $\sim 2 \times 10^9$ to $2 \times 10^{11} M_\odot$, and from the right panel, we see that both rotation and dispersion-dominated galaxies are widely distributed.

2.3. Determination of Galaxy Properties for the SINS/ zC -SINF sample

Stellar masses, star formation rates and stellar ages are derived from SED modeling of broad-band photometry in Förster Schreiber et al. (2009), Mancini et al. (2011) and Förster Schreiber et al. (2011) and assume either constant star formation histories or exponentially declining models with Bruzual & Charlot (2003) tracks. The ages are highly uncertain and should be interpreted in the sense that the bulk of galaxy light comes from stars younger than this “age”, and as such are best used as relative and not absolute ages. The star formation rates are taken as an average of those calculated from SED modeling and $\text{H}\alpha$ -based star formation rates, derived using $\text{SFR} = L(\text{H}\alpha) / (2.1 \times 10^{41} \text{ erg/s}) (M_\odot \text{yr}^{-1})$ (Kennicutt 1998, corrected for a Chabrier (2003) IMF), where $L(\text{H}\alpha)$ is extinction corrected based on the Calzetti et al. (2000) reddening law with $A_{V,gas} = 2.3 \times A_{V,SED}$. Förster Schreiber et al. (2009) and Wuyts et al. (2011) have shown that an extra attenuation factor of ~ 2.3 is a good representation of the global extinction towards HII regions relative to the bulk of starlight for $z \sim 2$ SFGs.

We calculate molecular gas masses (M_{gas}) and surface densities ($\Sigma_{gas} = 0.5 \times M_{gas} / (\pi(R_{1/2})^2)$) from the $\text{H}\alpha$ - and SED-derived SFRs using the star formation rate/molecular gas mass relation calibrated from the IRAM Large Program of CO in $z \sim 1-2$ SFGs ($t_{depl} = 1.5 \times (1+z)^{-1}$ Gyr, Tacconi et al. 2012). This simple linear relation has been shown to hold for both local and high- z SFGs, yielding $M_{gas}(M_\odot) = t_{depl} \times \text{SFR}(M_\odot/\text{yr})$

TABLE 1
 SOURCE SELECTION

Dataset	z	Galaxies	AO?	Instrument	Reference
SINS/zC-SINF	1.5–2.5	34	AO	SINFONI/VLT	this paper ¹
SINS/zC-SINF	1.5–2.5	4	seeing-lim.	SINFONI/VLT	Förster Schreiber et al. (2009) ²
BX/BM-selected	1.5–2.5	15	AO	OSIRIS/Keck	Wright et al. (2007, 2009); Law et al. (2009, 2012c) ³
Wiggle-Z	1.3–1.45	12	AO	OSIRIS/Keck	Wisnioski et al. (2011)
HiZELS	1.4–1.5	5	AO	SINFONI/VLT	Swinbank et al. (2012a,b)
MASSIV	1.2–1.4	3	AO	SINFONI/VLT	Epinat et al. (2012); Contini et al. (2012) ⁴
MASSIV	1–1.6	8	seeing-lim.	SINFONI/VLT	Lemoine-Busserolle & Lamareille (2010) and Epinat et al. (2012); Contini et al. (2012)

¹ Seeing-limited data of all of these galaxies has been presented in Förster Schreiber et al. (2009) and Mancini et al. (2011). Data of 9 of these galaxies have been presented in Genzel et al. (2006, 2011); Cresci et al. (2009); Förster Schreiber et al. (2009); Newman et al. (2012a), although 5 of these now contain new observations. The full AO data set will be described in detail in the forthcoming Förster Schreiber et al. (2013).

² New analysis of this data is presented here.

³ 3 galaxies from this sample were not included as they overlap with the SINS/zC-SINF sample.

⁴ These galaxies were selected from the total sample such that they had kinematic information based on the H α line from either H- or K-band, as the AO system on the VLT does not work as well in the J-band.

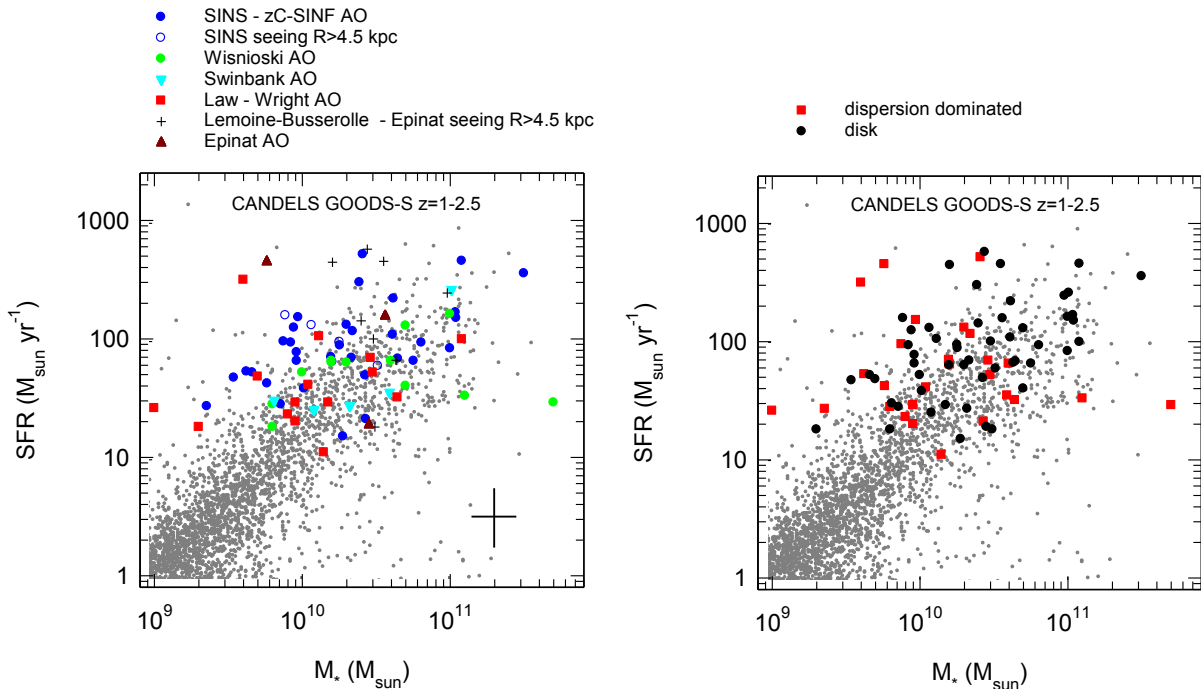


FIG. 1.— The star-formation rate/stellar mass plane. The grey points are from $z = 1-2.5$ galaxies from the CANDELS survey in the GOODS-S field. The left panel shows the distribution of galaxies from different parent samples used in our analysis. The blue closed (and open) circles are from the SINS/zC-SINF galaxies presented in this paper observed in AO (seeing-limited) mode. The red squares are from Law et al. (2009, 2012c); Wright et al. (2009), the cyan inverted triangles are from the SHiZELS survey presented in Swinbank et al. (2012a,b), the maroon triangles denote the AO galaxies from Epinat et al. (2012), the green circles represent the AO data from the WiggleZ survey (Wisnioski et al. 2011), and the black '+'s denote galaxies from Epinat et al. (2012) and Lemoine-Busserolle & Lamareille (2010) that have $R_{1/2} > 4.5$ kpc and were observed in seeing-limited mode. The right panel shows the same distribution of galaxies according to their identification as dispersion- or rotation-dominated. Here, black circles represent galaxies determined to be rotation dominated, and red squares denote galaxies determined to be dispersion-dominated. Note that wherever possible, we used averages of the H α - and SED-derived SFRs.

(Bigiel et al. 2008; Tacconi et al. 2010, 2012; Saintonge et al. 2012) down to ~ 1 kpc scales, with scatter in the relation of ~ 0.3 dex due to the variation in slope and normalization from various studies and also intrinsic scatter in the relation (see: Genzel et al. 2010; Daddi et al. 2010b; Tacconi et al. 2012). The dynamical mass is calculated as, $M_{dyn} = 2R_{1/2}(v_{rot}^2 + 3.4 \times \sigma_0^2)/G$, where v_{rot} is the inclination-corrected rotation velocity and σ_0 is the in-

trinsic galaxy dispersion. The factor of 3.4 accounts for pressure support (asymmetric drift) in an exponential distribution.

Inclinations were determined from the minor axis to major axis ratio of the H α surface brightness distribution. We found overall good agreement between the morphological axes and those determined from kinematics, however smaller objects tended to exhibit a large

scatter in the position angles determined from the two methods. In addition, some of the larger, more face-on systems have their axis ratios and position angles partially affected by small-scale regions of enhanced surface brightness. Following Law et al. (2012a), we considered the intrinsic z -thickness of high- z SFGs in deriving $\sin(i)$ (assuming $\langle z \rangle / \langle R \rangle = 0.2$), although the inferred inclinations are not significantly different from those in the thin disk approximation. This technique assumes that the light distribution is intrinsically circularly symmetric. However, Law et al. (2012a) find fewer $b/a \sim 1$ systems than expected for a population of randomly oriented inclined disks. Wuyts et al. (in prep.) find the same trend at all z from 0 to 2, although with lower amplitude at lower redshift. Independent of whether this deviation from circular symmetry in the light distribution is due to an intrinsically triaxial light or matter distribution or whether it's due to the distribution of clumps distorting the symmetry, this results in additional uncertainties in our derived inclinations, mainly for face-on systems.

Intrinsic (corrected for the spatial resolution) half-light radii are based on 2D exponential profile (i.e. Sersic profile with index $n = 1$) fits to the $H\alpha$ surface brightness distributions using the code GALFIT (Peng et al. 2002) following the methodology described by Förster Schreiber et al. (2011) (details for the present SINS/zC-SINF AO sample are given by Förster Schreiber et al. (2013)). For six cases (BX389, BX482, GMASS-2540, ZC405501, ZC406690, and ZC410041), a Gaussian profile (Sersic $n = 0.5$) was found to provide a significantly better representation of the data and we adopted the sizes derived from these Gaussian fits. Sersic profiles with $n \lesssim 1$ are motivated by the previous analysis of a subset of six SINS galaxies (Förster Schreiber et al. 2011), and the more recent result from a larger sample of $z \sim 1.5$ SFGs by Nelson et al. (2012).

The oxygen abundances are derived from the observed $[\text{NII}]/H\alpha$ flux ratio using the Pettini & Pagel (2004) calibration: $12 + \log_{10}(\text{O}/\text{H}) = 8.90 + 0.57 \times \log_{10}([\text{NII}]/H\alpha)$. This calibration is most often used for high- z galaxies with emission line data of only $H\alpha$ and $[\text{NII}]$, and thus we choose it for simplicity of comparison with previous work. We note that there are several uncertainties associated with this particular calibration (see e.g., Kewley & Ellison 2008), so it is taken as a relative measure of gas-phase abundance among our objects.

2.4. Determination of Kinematic Properties

For each galaxy, we computed the observed velocity gradient (Δv_{grad}) as the maximum velocity difference across the source from the velocity map produced from the data cube. The total Gaussian line width integrated over the source (σ_{tot}) is calculated from the width of the $H\alpha$ line from the spatially integrated spectrum for each galaxy. For SFGs with a substantial component of rotation or large-scale orbital motion, σ_{tot} is strongly affected or even dominated by beam-smearing rotation. However, all of the SINS/zC-SINF galaxies presented in this paper are resolved well enough in either the AO or seeing-limited data to estimate the average intrinsic local velocity dispersion (σ_0) from the velocity dispersion maps, and we minimize the effects of beam smearing by measuring the observed velocity dispersion in the outer parts of the source. Note that all quoted velocity disper-

sions have been corrected for the instrumental response function and are thus intrinsic quantities of the source. We determine the rotational velocity (v_{rot}) by correcting Δv_{grad} for our best-fit inclination.

In determining the kinematic properties for the other galaxies in our larger sample, we attempt to use as consistent a method as possible. Epinat et al. (2012) and Lemoine-Busserolle & Lamareille (2010) use a similar method to ours for determining v_{rot} and σ_0 , so we use the values presented in their papers. As with our method, they create maps of the velocity and dispersion fields for their galaxies that are corrected for instrumental resolution and additionally subtract (in quadrature) a beam-smearing component as estimated from thin rotating-disk models. Davies et al. (2011) has shown that deriving kinematic parameters from such modeling has the advantage of not being systematically biased by beam smearing and most often produces more correct results. However, there can be some inaccuracy in the resulting parameters due to low S/N, and Davies et al. (2011) suggest that extracting σ_0 from the outer regions of the galaxy (as we do with the SINS/zC-SINF galaxies) could help alleviate this issue. Either way, these two techniques should provide similar results. For the SHIZELS galaxies from Swinbank et al. (2012a), we take v_{rot} and σ_0 from their Figure 4, assuming the values in the outer regions of the galaxies, for consistency with our method. We note the the values they give for σ are almost all larger than the ones we assume. This is consistent with the bias towards higher σ_0 values demonstrated by Davies et al. (2011), which is found when correcting for beam smearing without generating disk models or without ignoring the central regions of the galaxy. We do the same for the Wright et al. (2009) galaxies, using their velocity and velocity dispersion maps. For the Law et al. (2009, 2012c) galaxies, we take their v_{rot} and σ_0 values, which were derived from fitting a Gaussian to the line profile from each pixel and flux-weighting to determine an average. As mentioned in their work and Davies et al. (2011), this produces an upper-limit for σ_0 once beam-smearing is accounted for, and this is reflected in Figures 5 through 9. Wisnioski et al. (2011) do not derive σ_0 values in a way that is comparable to our values, so we use their dataset for v_{rot} comparison only.

We follow Förster Schreiber et al. (2009) and operationally define dispersion dominated and rotation dominated SFGs as having $\Delta v_{grad}/2\sigma_{tot} < 0.4$ and ≥ 0.4 , respectively, for both AO and seeing-limited data. This operational divide is based on disk models of masses and sizes roughly spanning the range observed in our sample and with typical beam-smearing of seeing-limited data. Once corrected for inclination and beam smearing, it closely corresponds to the more intuitive physical definition $v_{rot}/\sigma_0 < 1$ and ≥ 1 . None of the galaxies in our sample are obvious major mergers but several may be minor mergers with a kinematically related companion galaxy within 10–20 kpc. For these, we consider the kinematic properties of the entire system.

We caution that a detection of a velocity gradient is certainly required but is by itself not sufficient to prove that a galaxy is rotating. If the velocity gradient is along the morphological major axis and at the same time, a peak of velocity dispersion is present near the morphological centroid, the evidence becomes more convincing.

This second line of evidence is present for most of the galaxies in the SINS/zC-SINF sample. The ultimate, but hardest, criterion is the detection of a symmetric ‘spider diagram’ pattern in the iso-velocity contours whose shape/curvature is consistent with the inclination estimated from the minor to major axis ratio (van der Kruit & Allen 1978). This most demanding proof is not reached by any of the compact dispersion dominated systems, and only by very few of the large disks/rings.

3. THE NATURE OF DISPERSION DOMINATED SFGS

As discussed in the Introduction, all investigations of the spatially resolved ionized gas dynamics have consistently found that $z\sim 1-3$ SFGs possess large internal random motions, in addition to large scale ordered velocities, such as rotation (in a disk), or orbital motion (in an interacting or merging system). In a significant fraction (anywhere from 20-90%, depending on the sample and definition of kinematic parameters) of the available IFU samples, the random motion component even appears to dominate, similar to what is seen in spheroidal galaxies. This characteristic feature of high- z galaxies is surprising, since in a gas rich system, supersonic turbulence should dissipate on a dynamical time scale ($\sim 10^{7-7.5}$ yr), unless it is continuously replenished.

3.1. Dispersion Dominated Galaxies are Small

Figure 2 shows postage stamps of the velocity-integrated H α emission maps of 34 of the SINS and zC-SINF AO data sets. The galaxies are ordered such that the 17 galaxies in the top two rows have $\Delta v_{grad}/2\sigma_{tot}$ below or very near 0.4, and are thus classified as ‘dispersion dominated’ based on the seeing limited data of Förster Schreiber et al. (2009); Mancini et al. (2011). According to the same criterion, the other 17 galaxies in Figure 2 are rotationally supported. None of the 34 is an obvious major merger, but the presence of a spatially well-separated secondary component in six of these SFGs (BX543, BX513, zC409985, zC410041, zC407376, zC407302) may be evidence for an ongoing minor merger (mass ratio $>3:1$), although in some cases it is difficult with the data in hand to distinguish unambiguously between bright clumps in large disks and minor merger systems.

Figure 2 immediately shows that the most obvious characteristic of dispersion dominated systems is their small size. If we look at those galaxies with $R_{1/2} \leq 3$ kpc, then most of these 13 smaller systems fulfill one or several of the kinematic definitions of dispersion dominated galaxies as introduced in Section 2.4,

$$(\Delta v_{grad}/(2 \times \sigma_{tot}))_{seeing} \leq 0.4 \quad (1)$$

$$(\Delta v_{grad}/(2 \times \sigma_{tot}))_{AO} \leq 0.4 \quad (2)$$

$$v_{rot}/\sigma_0 \leq 1 \quad (3)$$

Comparison of seeing limited (FWHM $\sim 0.56''$) and AO-scale (FWHM $\sim 0.20''$) data of the same galaxies shows that the classification as dispersion or rotation dominated can depend strongly on angular resolution. This is demonstrated in Figures 3 and 4, which show the velocity and velocity dispersion fields for Q1623-BX455

and GMASS-2363 in both seeing and AO modes. As the galaxies are small ($R_{1/2} \sim 0.2''$), the seeing limited data (resolution $\sim 0.5''$) do not resolve them and appear to confirm their dispersion dominated classification. However, with the AO data (resolution $\sim 0.2''$), both galaxies appear to be inclined rotating disks, based on the first two criteria for rotation outlined at the end of section 2 (velocity gradient along the morphological major axis and peak in velocity dispersion near the morphological center), yet like most high- z galaxies, neither exhibit the ‘spider diagram’ required for a more definitive proof.

3.2. Impact of Resolution on Kinematic Classification

In order to explore the impact of instrumental resolution on the classification (scenario 2 from Section I) of galaxies as dispersion- or rotation-dominated, we used the sample of 34 SINS/zC-SINF galaxies, for which we have both seeing limited and AO resolution data, taken with the same instrument and analyzed with the same tools. We compare the location of these galaxies in the $\Delta v_{grad}/(2 \times \sigma_{tot})$ vs. $R_{1/2}$ plane in Figure 5 for both seeing-limited data (left panel) and AO data (middle panel). The shift to higher $\Delta v_{grad}/(2 \times \sigma_{tot})$, and thus more rotation-dominated classification, with higher resolution data is clear. We also show our entire sample in the v_{rot}/σ_0 versus $R_{1/2}$ plane in the right panel.

It is apparent that for all IFU data sets the dispersion dominated classification correlates with the intrinsic source size (smaller galaxies are more likely dispersion dominated), although they are not perfectly matched. But as we see from the first two panels, this classification also depends on the ratio of resolution to source size, such that poorly resolved galaxies are very likely classified as dispersion dominated. Given the criteria above, formally 41% of the 34 SINS/zC-SINF galaxies are classified as dispersion dominated based on seeing limited data. That fraction drops to 6–9% for the same galaxies using AO data. If we include 1σ error bars, up to 59% of the galaxies could be classified as dispersion dominated with seeing limited data and less than 35% with AO data.

In turn, the strong majority of the SINS/zC-SINF SFGs observed with AO can then be characterized by a velocity gradient along a single axis that is identical with or close to the morphological major axis. This suggests that rotation dominates the larger scale velocity field, although the observed pattern could also be matched by orbital motion in a binary minor merger in a few cases. However, we do not detect symmetric double light distributions or velocity reversals in any of the SFGs in our sample, which would be indicative of a major merger.

The empirical assessment drawn from Figure 5 is supported by creating simple toy models of turbulent but rotationally supported disks with intrinsic $v_{rot}/\sigma_0 \sim 1-5$. We ‘observe’ model disks with varying sizes, masses and inclinations with seeing and AO scale resolutions and analyze them in the same way as our SINS/zC-SINF data. Their location in the empirical $\Delta v_{grad}/2\sigma_{tot} - R_{1/2}$ and $v_{rot}/\sigma_0 - R_{1/2}$ planes overlaps with the majority of the data. A fraction of the model disks indeed come to reside in the locus of ‘dispersion dominated’ galaxies, although they are intrinsically rotationally supported.

Finally, we carry out weighted linear fits to the data in log-log space (i.e. $\log(v_{rot}/\sigma_0)$ vs. $\log(R_{1/2})$) and calcu-

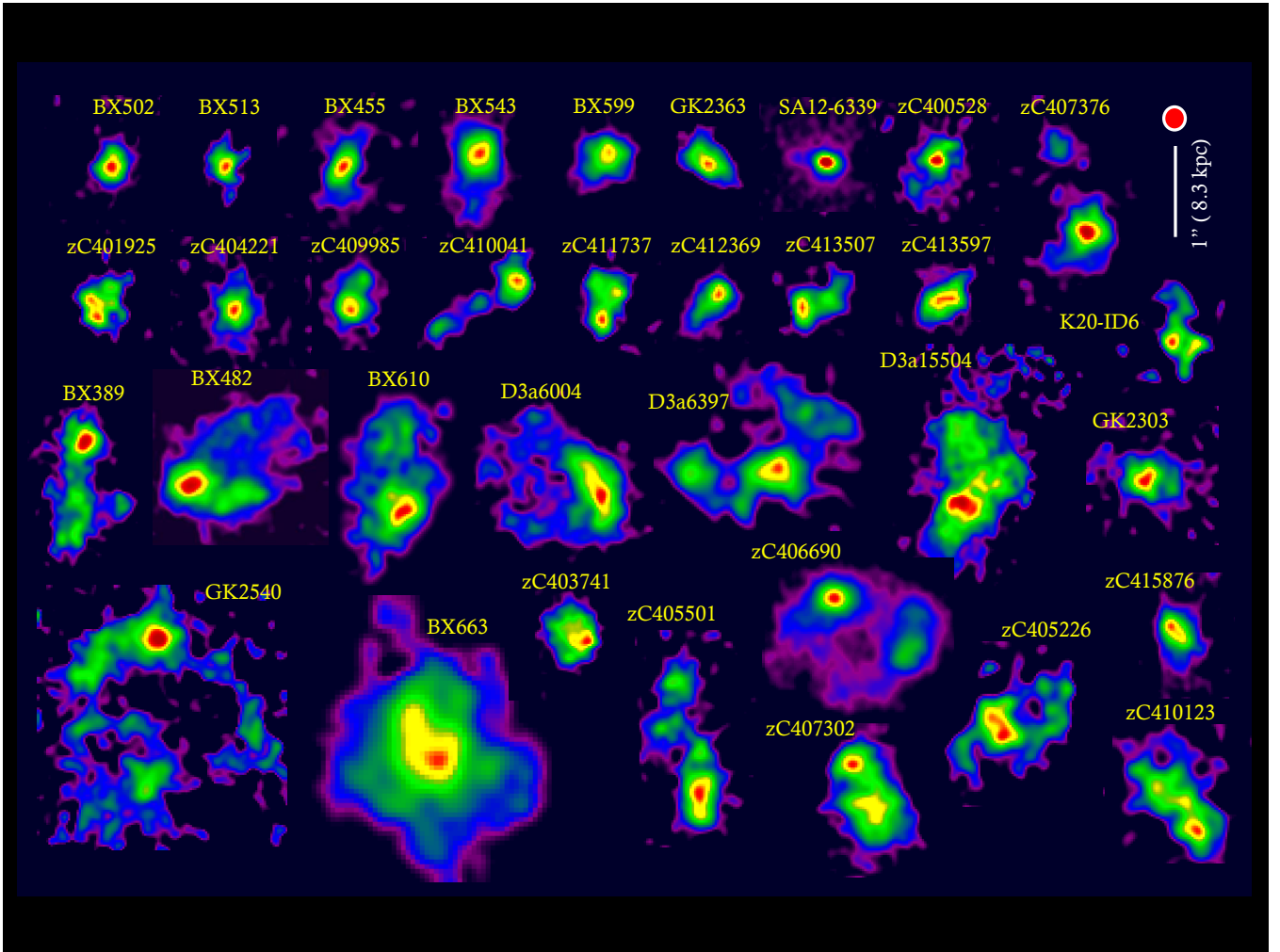


FIG. 2.— Integrated $H\alpha$ maps in AO mode (0.2–0.3'' FWHM) of the 34 SFGs in our (AO) sample. The top two rows contain the dispersion dominated SFGs (as defined by the criterion $(\Delta v_{grad}/(2\sigma_{tot}))_{seeing} \leq 0.4$, Förster Schreiber et al. (2009)), and the rest are rotation dominated. The maps were interpolated on a pixel scale of 0.025'' and are all plotted on the same angular scale. The typical FWHM resolution is shown as a red circle. The dispersion dominated galaxies tend to be more compact than the rotation dominated galaxies with the peak of their $H\alpha$ emission in the center.

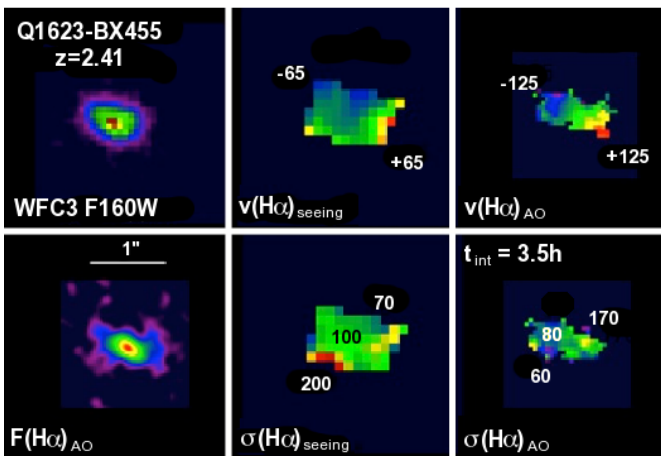


FIG. 3.— Top row, left to right: HST WFC3 (Law et al. 2012a) image, seeing-limited velocity field, AO velocity field. Bottom row, left to right: $H\alpha$ AO image, seeing-limited velocity dispersion field and AO velocity dispersion field of Q1623-BX455 (Förster Schreiber et al. 2009). Much of the rotation apparent from the AO velocity field is beam-smearred out with the seeing-limited data.

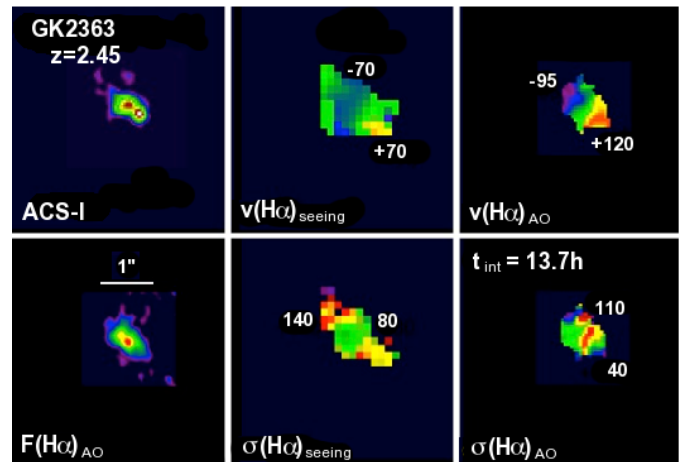


FIG. 4.— Top row, left to right: HST ACS I-band image, seeing-limited velocity field, AO velocity field. Bottom row, left to right: $H\alpha$ AO image, seeing-limited velocity dispersion field and AO velocity dispersion field of GMASS-2363 (Förster Schreiber et al. 2009).

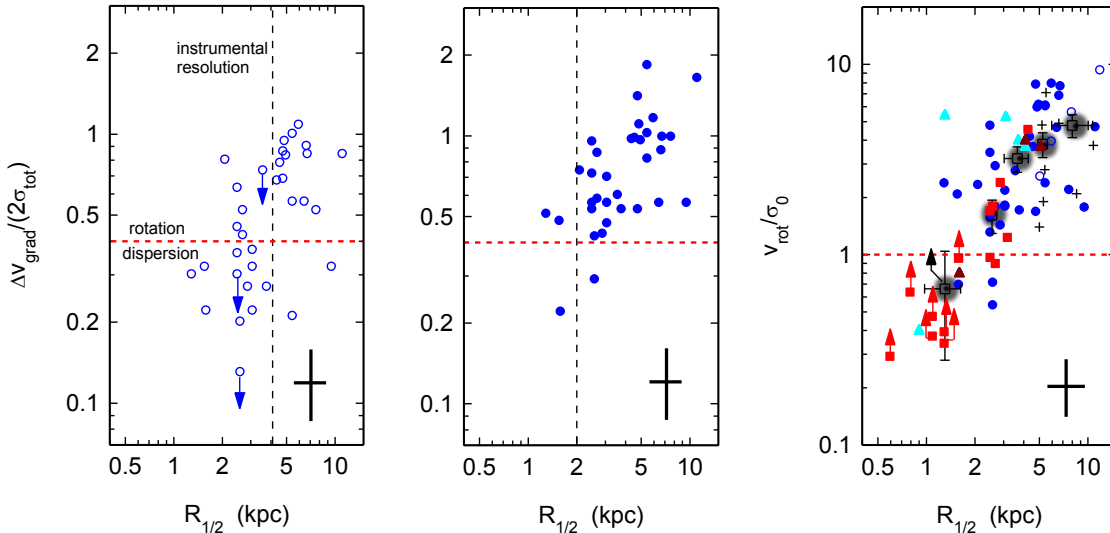


FIG. 5.— Dependence of the ratio of rotation to dispersion on the half light source radius ($R_{1/2}$) and resolution. Left panel: seeing-limited SINS/zC-SINF data (Förster Schreiber et al. 2009; Mancini et al. 2011). Middle panel: AO SINS/zC-SINF data (this paper and Förster Schreiber et al. 2013). Right panel: Combined AO and seeing-limited data for galaxies that have sufficient angular resolution for dynamical modeling to obtain the inclination corrected v_{rot} and the beam smearing corrected σ_0 (i.e. all galaxies with AO data and seeing-limited only galaxies with $R_{1/2} > 4.5$ kpc). The colored symbols are the same as for the left panel of Figure 1. Grey filled circles denote the median-binned values in four radius bins with horizontal error bars representing the standard deviation in the bins and vertical error bars representing the 1σ uncertainty. Many of the same galaxies are plotted in all three panels (for the SINS data). The horizontal dashed red lines mark the operational divide between dispersion and rotation dominated SFGs for the corresponding criteria for each panel. The vertical dashed black lines in the left and middle panels mark the FWHM spatial resolution of the data. Typical 1σ error bars for individual measurements are plotted at the bottom of each panel. Many of the galaxies characterized as dispersion dominated according to the seeing-limited data (left panel), would be considered rotation dominated with the higher-resolution AO data (middle panel) or with full dynamical modeling (right panel), and an important factor in the kinematic classification is the ratio of the galaxy size to the instrumental resolution.

TABLE 2
SIGNIFICANCE OF CORRELATION WITH KINEMATIC PARAMETERS

Parameter 1	Param. 2	Lin. Slope of Fit	Sign. ¹	See Fig.:
$\log(v_{rot}/\sigma_0)$	$\log(R_{1/2})$	0.77 ± 0.12	6.4	5
$\log(v_{rot})$	$\log(R_{1/2})$	0.62 ± 0.094	6.6	6
$\log(\sigma_0)$	$\log(R_{1/2})$	-0.14 ± 0.05	2.8	6
$\log(M_{dyn})$	$\log(v_{rot}/\sigma_0)$	1.19 ± 0.097	12.3	7
$\log(M_*)$	$\log(v_{rot}/\sigma_0)$	0.54 ± 0.14	3.9	7
$\log(f_{gas})$	$\log(v_{rot}/\sigma_0)$	-0.028 ± 0.05	0.56	8
$12+\log(O/H)$	$\log(v_{rot}/\sigma_0)$	0.1 ± 0.046	2.2	8
$\log(\Sigma_{SFR})$	$\log(v_{rot}/\sigma_0)$	-0.89 ± 0.18	4.9	9

¹ Significance of best fit linear slope as opposed to slope of 0.

late the formal significance of the slope differing from 0. The resulting best-fit slope and significance for data in the right panel of Figure 5 (and the remaining Figures) is presented in Table 2.

A similar dependence of kinematic classification on resolution was discussed in Jones et al. (2010) (see also: Gonçalves et al. 2010). They found that without the boost in spatial resolution provided by gravitational lensing, many of the galaxies that they identified as rotating disks would not be distinguishable from mergers or dispersion dominated sources based on their velocity profiles, even with the use of AO. However, we caution that our sources are generally much larger than those in the Jones et al. (2010) work ($\langle R_{1/2} \rangle \sim 2$ kpc), and will thus suffer less beam smearing with the use of AO even without the added spatial resolution of gravitational lensing.

3.3. Why Are Small Galaxies More Likely to be Dispersion Dominated?

The last section has shown that resolution effects can make an intrinsically rotation dominated system appear to be dispersion dominated if it is small, especially with seeing limited data. However, the middle and right panels of Figure 5 show that $\Delta v_{grad}/(2\sigma_{tot})$ and v_{rot}/σ_0 increase with radius even for well-resolved data sets, and even at AO resolution, there remain a number of dispersion dominated SFGs, for which the classification cannot be an instrumental effect. What causes this intrinsic dependence on size?

In Figure 6, we plot the rotation velocity (corrected for inclination) and the intrinsic velocity dispersion (corrected for beam-smearing) as a function of $R_{1/2}$. Rotation velocity increases strongly with $R_{1/2}$ but there is no strong trend with velocity dispersion and the running median suggests that σ_0 is constant or perhaps slightly decreasing with $R_{1/2}$. The best fit weighted power law to the data in Figure 6 yields $v_{rot} = 59(\pm 13) \times R^{0.73(\pm 0.18)}$, but a linear slope is also consistent with the data within the 2σ fit error, which would be physically motivated by centrifugally supported baryonic disks of constant angular momentum parameter embedded in a virialized dark matter halo (Mo et al. 1998). Figure 6 thus shows that small galaxies are intrinsically more likely to be dispersion dominated because of the near-constant value of the local velocity dispersion in all high- z SFGs, which may suggest a velocity dispersion floor. Such a floor ($\langle \sigma_0 \rangle$

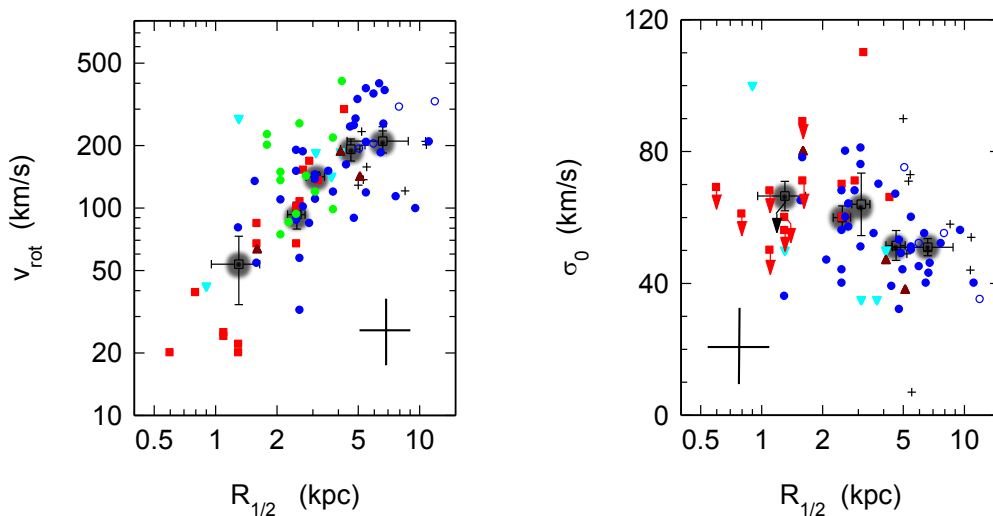


FIG. 6.— Dependence of v_{rot} (left panel) and σ_0 (right panel) on $R_{1/2}$. The data symbols are the same as in Figures 1 and 5. The strong trend in the left panel can be well fit by a linear relation: $\log(v_{rot}) = 0.62 (\pm 0.094) \times \log(R_{1/2}) + 1.9 (\pm 0.06)$ (see Table 2). In contrast, the right panel does not appear to show a significant trend, considering that many of the red data points (those from Law et al. (2009, 2012c)) are strictly upper limits to σ_0 . Thus the trend for smaller galaxies to be dispersion dominated is in part due to the combination of a possible floor of velocity dispersion, and a linear increase of rotation velocity with size. We note that the characteristic error bars do not include potential additional uncertainties due to deviations from circular symmetry. However, these uncertainties really only strongly influence near face-on systems, which are very few in this data set.

$\sim 60 \pm 10 \text{ km s}^{-1}$) may be caused by star formation feedback or by the dissipation of gravitational energy within and at the outer edge of the disk (Immeli et al. 2004a,b; Westmoquette et al. 2007; Bournaud et al. 2009; Agertz et al. 2009; Ceverino et al. 2010; Genzel et al. 2008, 2011; Genel et al. 2012b,a; Elmegreen & Burkert 2010; Krumholz & Burkert 2010).

3.4. Dependence on Stellar Mass, Gas Fraction and Age

Figure 7 shows that dispersion dominated galaxies tend to have smaller stellar and dynamical masses, in agreement with the earlier conclusions of Förster Schreiber et al. (2009); Law et al. (2009); Wisnioski et al. (2011); Epinat et al. (2012). From the right panel of Figure 1, we see that while the dispersion dominated population (on the AO scale) is mostly found toward lower stellar masses, there is still substantial overlap with the location of disks. Thus, it seems that the best separation between the two kinematic populations is in terms of size and dynamical mass.

Figure 8 shows that the gas fraction ($f_{gas} = (M_{mol-gas} / (M_{mol-gas} + M_*))$) may be correlated with v_{rot}/σ_0 , but that this trend becomes far more uncertain for the dispersion dominated objects. While there is a large range in gas fraction for the dispersion dominated objects, some have gas fractions as large as 90%, much higher than for most of the larger rotating disks. These gas fractions are larger than those found by Tacconi et al. (2012) based on CO observations from Plateau de Bure for a sample of massive ($M_* > 3 \times 10^{10} M_\odot$) SFGs at $z = 1.2$ and $z = 2.2$. This is likely because of a combination of the lower masses and above-main sequence location of many dispersion dominated galaxies (see right panel of

Figure 1). Tacconi et al. (2012) have shown that gas fractions increase with decreasing stellar mass and with increasing offset from the star-forming ‘main sequence’ in the stellar mass - SFR plane.

There is a modest difference in the strength of the [NII] line relative to the $H\alpha$ line between the dispersion and rotation-dominated sub-samples, implying a metallicity trend (see Figure 8). We stack the spectra of the SINS/zC-SINF galaxies by kinematic type, and find that the dispersion dominated sub-sample has $\langle F[\text{NII}] 6584 / F[H\alpha] \rangle = 0.13 (\pm 0.01)$, while the rotation dominated sub-sample has $\langle F[\text{NII}] 6584 / F[H\alpha] \rangle = 0.19 (\pm 0.01)$, consistent with the larger stellar masses of the rotation dominated sub-sample and the mass-metallicity relation (Tremonti et al. 2004; Erb et al. 2006; Mannucci et al. 2009). The errors here derive from the uncertainty in the fitting of the emission lines. These averages do not include the galaxies identified to contain AGN.

As found in Newman et al. (2012b), $z \sim 2$ SFGs with $\Sigma_{SFR} > 1 M_\odot \text{ yr}^{-1} \text{ kpc}^{-2}$ have evidence for strong outflows, based on the ratio of broad $H\alpha$ emission to narrow $H\alpha$ emission (which likely traces star-forming gas in the disk). We find that dispersion-dominated galaxies generally have higher Σ_{SFR} than the sample as a whole (Figure 9). When coupled with Figures 6 and 7, this suggests that outflows may be stronger (or more likely) in galaxies with smaller rotation velocities and dynamical masses (as suggested by theoretical models, e.g. Murray et al. 2005).

When comparing the mean ages of ‘rotation’ or ‘dispersion dominated’ galaxies from the SINS/zC-SINF sample we also see a relative trend. When classified using seeing-limited data, the dispersion dominated sample has a mean age of 460 Myr, while the rotation dominated galaxies have a mean age of 690 Myr. This contrast is

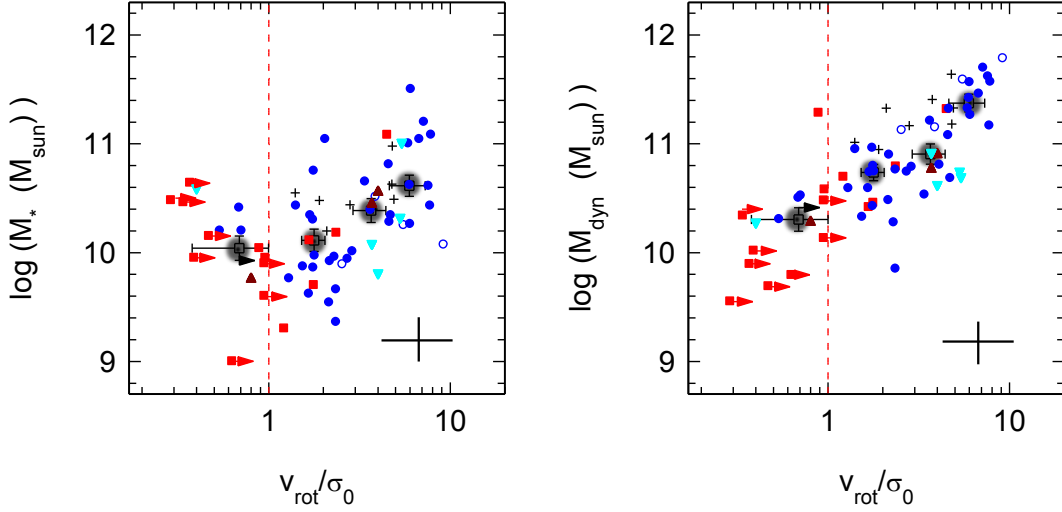


FIG. 7.— Dependence of stellar mass (left) and dynamical mass (right) on v_{rot}/σ_0 . Symbols are the same as in Figures 1, 5 and 6.

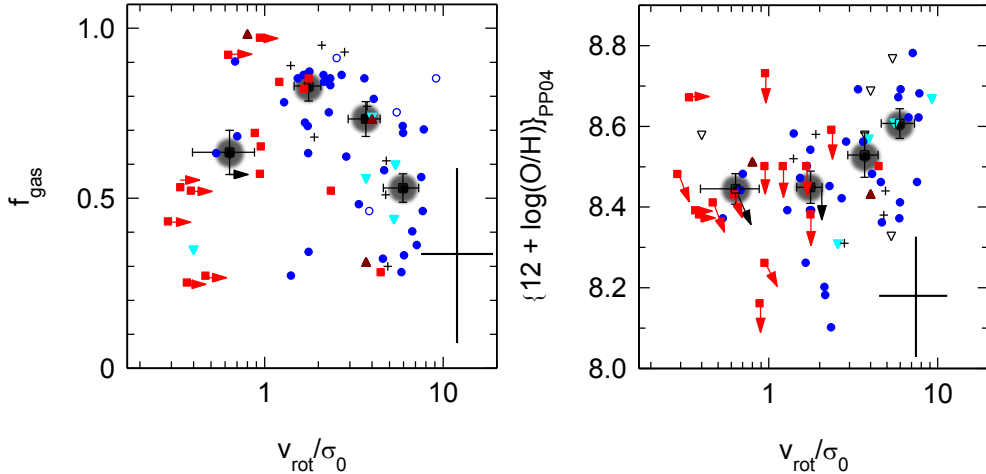


FIG. 8.— Dependence of baryonic gas fraction ($f_{gas} = (M_{mol-gas}/(M_{mol-gas} + M_*))$) (left panel) and gas phase oxygen abundance (right panel) on v_{rot}/σ_0 . Symbols are the same as in Figures 1 and 5 to 7. For the MASSIV sample, the gas masses and H α half-light radii are listed in Vergani et al. (2012) and the metallicities in Queyrel et al. (2012). Gas fraction and metallicity are correlated with kinematical type, such that dispersion dominated galaxies are more gas rich and slightly more metal poor.

even stronger when using AO data or the v_{rot}/σ_0 criteria, wherein the mean ages are 120 and 650 Myr for the dispersion and rotation dominated samples, respectively. These ages pertain to the stars providing the bulk of the rest-frame UV and optical radiation, as these dominate the photometry used in our SED analysis.

We thus find that high- z SFGs may be classified as ‘dispersion dominated’ for two main reasons, namely that (a) intrinsic rotation is beam-smearred by insufficient spatial resolution, and (b) the small galaxy size is accompanied by lower rotation velocity, which when coupled with the nearly constant floor of velocity dispersion leads to a low v_{rot}/σ_0 ratio. These conclusions enable us to reflect on the question posed in the Introduction about what these objects really are. We find that:

- (1) The dispersion dominated objects may indeed be an earlier evolutionary stage of larger disks due to the lower stellar and dynamical masses, lower metallicities and possibly higher gas fractions. We discuss this possibility in more detail in the following section.
- (2) It also appears that they are (smaller) rotating disks, with rotation that is masked by beam-smearing due to insufficient resolution in addition to intrinsically lower rotation velocities (likely due to their smaller dynamical masses).
- (3) A fraction of the dispersion dominated systems may also be the product of a recent major merger. While the parent samples from which our

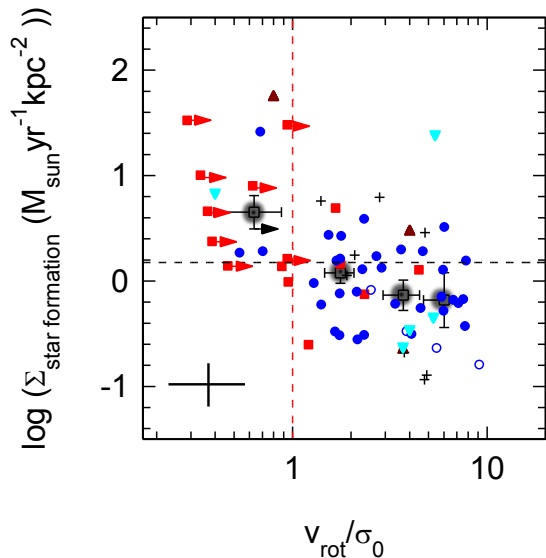


FIG. 9.— Dependence of star formation rate surface density ($\Sigma_{SFR} = 0.5 \text{ SFR}/\pi(R_{1/2})^2$) on v_{rot}/σ_0 . The symbols are the same as in Figures 1 and 5 to 8. The threshold for strong $z \sim 2$ galactic-scale outflows observed by Newman et al. (2012b) and marked by the black dashed line is at $\Sigma_{SFR} \sim 1.5 \text{ M}_\odot \text{ yr}^{-1} \text{ kpc}^{-2}$.

SFGs were drawn already only contained a few binary systems with kinematic properties consistent with major mergers (which we have intentionally excluded, see methods of e.g. Shapiro et al. 2008; Förster Schreiber et al. 2009), and the new AO observations discussed here have not uncovered new major merger candidates of somewhat smaller size, there could still be late stage major mergers in our sample masquerading as dispersion dominated if they are sufficiently compact.

(4) It is less likely that the dispersion dominated objects are merely large clumps in low surface brightness disks. First, if this were the case, we would not expect to see more rotation with higher spatial resolution. In addition, when we stack all of the galaxies classified as dispersion dominated based on seeing-limited data, we find sersic indices of ~ 0.5 – 1 with $r_{eff} \approx \langle R_{1/2} \rangle$, and without excess extended emission. Law et al. (2012a) also find that a stack of their ‘Type I’ galaxies is well fit by an $n \sim 1$ sersic profile, with $r_{eff} = 1.36 \text{ kpc}$.

4. IMPLICATIONS FOR GALAXY EVOLUTION

Based on this combined sample of IFU datasets, we are able to hypothesize on how the dispersion dominated galaxies affect our picture of galaxy evolution. Our finding that most of these galaxies are both highly gas-rich and rotating (albeit smaller and more slowly than the larger disks) systems, naturally leads to an explanation of their formation in the context of gravitational instabilities in gas rich disks. If we frame the Toomre (or Jeans) mass in terms of gas fraction and v/σ , we find that for a marginally stable disk with $Q \sim 1$, that $R_{toomre} \sim$

$R_{disk} \times (\sigma/v)$ (Genzel et al. 2011). Genzel et al. (2011) used this argument to explain why $R_{1/2} \sim 5 \text{ kpc}$ disks form $\sim 1 \text{ kpc}$ clumps, however, this can also be used to show that for the dispersion-dominated galaxies (with $v_{rot}/\sigma_0 \sim 1$), ‘clumps’ will naturally form on the scale of $R_{1/2}$ (or $\sim 2 \text{ kpc}$). Thus in the same scenario in which clumps form in extended, gravitationally-unstable disks, the dispersion dominated galaxies will essentially form one giant highly-unstable clump.

In addition to the smaller sizes and potentially higher gas fractions, we also found that dispersion dominated galaxies tend to have lower stellar masses, younger ages (based on SED fitting), and lower inferred metallicities on average than rotation dominated galaxies. One can imagine a scenario in which the smaller dispersion-dominated galaxies are ‘seeds’ for the larger and more massive rotating disks, and these larger galaxies at $z \sim 2.2$ have merely evolved sooner. As these ‘seeds’ continue to rapidly accrete gas, form stars and expel winds, they also grow in size, build up their stellar masses, increase in metallicity and decrease in gas fraction. We find that these dispersion dominated galaxies are more likely to have star formation surface densities above the wind ‘break-out’ threshold proposed by Newman et al. (2012b) than their larger disky counterparts, implying that they drive outflows more efficiently than the latter ones do (see also: Law et al. 2012b). The higher stellar masses will eventually stabilize the disks, and the larger sizes and increased rotation velocities will decrease the Toomre scale, shrinking the size of the star-forming regions (the clumps). A similar mechanism for the growth of dispersion-dominated galaxies into rotationally-supported disks was also suggested by Law et al. (2012b). We note that our dispersion-dominated galaxies are on average not the same as the high- z compact star-forming galaxies (‘blue nuggets’) recently reported on by Barro et al. (2013), which they propose will soon quench and become compact quiescent galaxies. While two of the galaxies from our sample (BX502 and SA12-6339) do meet their mass/size criteria, the remainder of our smaller galaxies have much lower stellar masses (by a factor of ~ 2 – 5).

The picture we have presented, in which stellar mass builds up in the centers of galaxies through this ‘compact dispersion-dominated’ phase is supported by additional observational evidence. Based on 3D-HST $H\alpha$ and rest-frame R-band data of $z \sim 1$ SFGs, Nelson et al. (2012) find that $H\alpha$ emission is typically more extended than continuum emission, but that this is less often the case for the smallest objects ($r_{H\alpha} < 3 \text{ kpc}$) that have star formation surface densities $> 1 \text{ M}_\odot \text{ yr}^{-1} \text{ kpc}^{-2}$, suggesting inside-out growth. Similarly, Wuyts et al. (2012) find that $z \sim 1$ – 2 SFGs from the CANDELS survey typically have large stellar bulges with high extinction and/or old stellar ages and UV-bright star-forming clumps with little or no excess in stellar mass at outer radii.

These unstable $z \sim 2.2$ galaxies will grow until they are ‘mass quenched’ with increasing probability as they grow in mass beyond the Schechter mass of $\sim 10^{10.7-11} \text{ M}_\odot$ (Conroy & Wechsler 2009; Peng et al. 2010), which requires a tripling of mass based on the median stellar mass of the galaxies in our sample. Given an average specific star formation rate of $\sim 2 \text{ Gyr}^{-1}$, this process

would take around 1.3 Gyr. Thus the most massive of our $z \sim 2.2$ SFG sample will be effectively quenched by $z \sim 1.5$. Indeed, highly unstable and morphologically disturbed SFGs are more rarely seen at this later epoch (Kassin et al. 2012), also owing to the fact that galactic gas accretion has slowed by this time (Birnboim et al. 2007). The remainder may evolve into L^* galaxies, as suggested by Conroy et al. (2008).

Another possibility for the evolution of dispersion dominated objects is that they are the product of clump migration and coalescence at the centers of larger disks, and are therefore the descendants of rotation dominated galaxies. However, if the clumps are formed by gravitational instability, we would expect them to be continuously produced in the unstable, gas-rich disks, and we should see some brighter emission outside the center of the dispersion dominated galaxies. In addition, this scenario is at odds with the lower stellar masses, younger ages and lower metallicities of the dispersion dominated systems. Indeed, one would expect that the first galaxies to experience clump coalescence would be the most massive rather than the least massive ones.

5. CONCLUSIONS

This paper presents, for the first time, a side-by-side comparison of high quality deep AO and seeing-limited kinematic data of the same galaxies for a larger number of objects. We note that this unprecedented data leads us to similar conclusions as those made in previous work. Based on IFU data of 81 star forming galaxies at $z=1-2.5$, we compare the sub-samples of galaxies known as dispersion and rotation dominated. We find that the characterization of a galaxy into one of these kinematic groups is a strong function of the galaxy size. Small galaxies are much more likely to fall in the category of dispersion dominated galaxies due to insufficiently resolved rotation

(especially with seeing-limited observations) and also as a result of the almost constant floor of velocity dispersion across all sizes paired with the linear increase of rotation velocity with size. Many galaxies that are considered dispersion dominated from more poorly resolved data actually show evidence for rotation with higher-resolution data.

Despite the finding that galaxies characterized as dispersion-dominated often show evidence for rotation with higher spatial resolution data, they have different average properties than rotation dominated galaxies. They tend to have lower stellar and dynamical masses, higher gas fractions, younger ages and slightly lower metallicities. We suggest that these galaxies could be precursors or ‘seeds’ to larger rotating galaxies, as they accrete more mass onto the outer regions of their disks. Our AO-based results provide important insights for the analysis and interpretation of seeing-limited IFU data, such as will become available for large samples with KMOS, through the quantitative assessment presented of the effects of beam-smearing on the observed kinematics of real galaxies.

We thank the referee for a detailed and thoughtful review which led to substantial improvements in the paper. We thank the ESO staff, especially those at Paranal Observatory, for their ongoing support during the many past and continuing observing runs over which the SINS project is being carried out. We also acknowledge the SINFONI and PARSEC teams, whose devoted work on the instrument and laser paved the way for the success of the SINS observations. SFN is supported by an NSF grfp grant. CM and AR and GZ acknowledge partial support by the ASI grant ‘‘COFIS-Analisi Dati’’ and by the INAF grant ‘‘PRIN-2008’’ and ‘‘PRIN-2010’’.

REFERENCES

- Abraham, R. G. et al. 2004, *AJ*, 127, 2455
 Adelberger, K. L., Steidel, C. C., Shapley, et al. 2004, *ApJ*, 607, 226
 Agertz, O., Lake, G., Teyssier, R., et al. 2009, *MNRAS*, 392, 294
 Aumer, M., Burkert, A., Johansson, P. H., & Genzel, R. 2010, *ApJ*, 719, 1230
 Barro, G., Faber, S. M., Perez-Gonzalez, P. G., et al. 2013, *ApJ*, 765, 104
 Bigiel, F., Leroy, A., Walter, F., et al. 2008, *AJ*, 136, 2846
 Birnboim, Y., Dekel, A., & Neistein, E. 2007, *MNRAS*, 380, 339
 Bonnet, H., Conzelmann, R., Delabre, B., et al. 2004, *Proc. SPIE*, 5490, 130
 Bouché, N. et al. 2007, *ApJ*, 671, 303
 Bournaud, F., Elmegreen, B. G., & Elmegreen, D. M. 2007, *ApJ*, 670, 237
 Bournaud, F., Elmegreen, B. G., & Martig, M. 2009, *ApJ*, 707, L1
 Bournaud, F., Elmegreen, B. G., Teyssier, R., Block, D. L., & Puerari, I. 2010, *MNRAS*, 409, 1088
 Bower, R. G., Benson, A. J., Malbon, R., et al. 2006, *MNRAS*, 370, 645
 Bruzual, G. & Charlot, S. 2003, *MNRAS*, 344, 1000
 Cacciato, M., Dekel, A., & Genel, S. 2012, *MNRAS*, 421, 818
 Calzetti, D., Armus, L., Bohlin, R. C., et al. 2000, *ApJ*, 533, 682
 Calzetti, D., Kinney, A. L., & Storchi-Bergmann, T. 1994, *ApJ*, 429, 582
 —. 1996, *ApJ*, 458, 132
 Cecil, G., Bland-Hawthorn, J., Veilleux, S., & Filippenko, A. V. 2001, *ApJ*, 555, 338
 Ceverino, D., Dekel, A., & Bournaud, F. 2010, *MNRAS*, 404, 2151
 Ceverino, D., Dekel, A., Mandelker, N., et al. 2012, *MNRAS*, 420, 3490
 Chabrier, G. 2003, *PASP*, 115, 763
 Chen, Y.-M., Tremonti, C. A., Heckman, T. M., et al. 2010, *AJ*, 140, 445
 Cid Fernandes, R., González Delgado, R. M., Storchi-Bergmann, T., Martins, L. P., & Schmitt, H. 2005, *MNRAS*, 356, 270
 Cimatti, A., Cassata, P., Pozzetti, L., et al. 2008, *A&A*, 482, 21
 Conroy, C., Shapley, A. E., Tinker, J. L., Santos, M. R., & Lemson, G. 2008, *ApJ*, 679, 1192
 Conroy, C. & Wechsler, R. H. 2009, *ApJ*, 696, 620
 Contini, T., Garilli, B., Le Fèvre, O., et al. 2012, *A&A*, 539, 91
 Cowie, L. L., Hu, E. M., & Songaila, A. 1995, *AJ*, 110, 1576
 Cresci, G. et al. 2009, *ApJ*, 697, 115
 Daddi, E., Bournaud, F., Walter, F., et al. 2010a, *ApJ*, 713, 686
 Daddi, E., Cimatti, A., Renzini, A., et al. 2004a, *ApJ*, 617, 746
 Daddi, E., Dannerbauer, H., Elbaz, D., et al. 2008, *ApJ*, 673, L21
 Daddi, E., Elbaz, D., Walter, F., et al. 2010b, *ApJ*, 714, L118
 Daddi, E. et al. 2004b, *ApJ*, 600, L127
 —. 2007, *ApJ*, 670, 156
 Davé, R. 2008, *MNRAS*, 385, 147
 Davies, R., Förster Schreiber, N. M., Cresci, G., et al. 2011, *ApJ*, 741, 69
 Davies, R. I. 2007, *MNRAS*, 375, 1099
 Dekel, A. & Birnboim, Y. 2006, *MNRAS*, 368, 2
 Dekel, A., Sari, R., & Ceverino, D. 2009, *ApJ*, 703, 785
 Eisenhauer, F., Abuter, R., Bickert, K., et al. 2003, *Proc. SPIE*, 4841, 1548
 Elmegreen, B. G., Bournaud, F., & Elmegreen, D. M. 2008, *ApJ*, 688, 67
 Elmegreen, B. G. & Elmegreen, D. M. 2005, *ApJ*, 627, 632
 —. 2006, *ApJ*, 650, 644
 Elmegreen, D. M., Elmegreen, B. G., Marcus, M. T., et al. 2009, *ApJ*, 701, 306
 Elmegreen, D. M., Elmegreen, B. G., & Sheets, C. M. 2004, *ApJ*, 603, 74
 Elmegreen, B. G. & Burkert, A. 2010, *ApJ*, 712, 294
 Epinat, B., Contini, T., Le Fèvre, O., et al. 2009, *A&A*, 504, 789
 Epinat, B., Tasca, L., Amram, P., et al. 2012, *A&A*, 539, A92

- Erb, D. K., Steidel, C. C., Shapley, A. E., et al. 2006, *ApJ*, 646, 107
- Fanelli, M. N., O’Connell, R. W., & Thuan, T. X. 1988, *ApJ*, 334, 665
- Feldmann, R., Gnedin, N. Y., & Kravtsov, A. V. 2012, *ApJ*, 758, 127
- Förster Schreiber, N. M., Shapley, A. E., Erb, D. K., et al. 2011, *ApJ*, 731, 65
- Förster Schreiber, N. M. et al. 2006, *ApJ*, 645, 1062
- 2009, *ApJ*, 706, 1364
- 2013, in prep.
- Genel, S., Naab, T., Genzel, R., et al. 2012a, *ApJ*, 745, 11
- Genel, S., Dekel, A., & Cacciato, M. 2012b, *MNRAS*, 425, 788
- Genzel, R., Newman, S., Jones, T., et al. 2011, *ApJ*, 733, 101
- Genzel, R., Tacconi, L. J., Gracia-Carpio, J., et al. 2010, *MNRAS*, 407, 2091
- Genzel, R. et al. 2006, *Nature*, 442, 786
- 2008, *ApJ*, 687, 59
- Gonçalves, T. S., Basu-Zych, A., Overzier, R., et al. 2010, *ApJ*, 724, 1373
- Heckman, T. M., Armus, L., & Miley, G. K. 1990, *ApJS*, 74, 833
- Hopkins, P. F., Quataert, E., & Murray, N. 2012, *MNRAS*, 421, 3522
- Immeli, A., Samland, M., Gerhard, O., & Westera, P. 2004a, *A&A*, 413, 547
- Immeli, A., Samland, M., Westera, P., & Gerhard, O. 2004b, *ApJ*, 611, 20
- Jones, T., Swinbank, A. M., Ellis, R. S., Richard, J., & Stark, D. P. 2010, *MNRAS*, 404, 1247
- Jones, T., Stark, D. P., & Ellis, R. S. 2012, *ApJ*, 751, 51
- Kassin, S. A., Weiner, B. J., Faber, S. M., et al. 2012, *ApJ*, 758, 106
- Kassin, S. A., Weiner, B. J., Faber, S. M., et al. 2007, *ApJ*, 660, L35
- Kennicutt, Jr., R. C. 1998, *ApJ*, 498, 541
- Kennicutt, Jr., R. C., Calzetti, D., Walter, F., et al. 2007, *ApJ*, 671, 333
- Kereš, D., Katz, N., Fardal, M., Davé, R., & Weinberg, D. H. 2009, *MNRAS*, 395, 160
- Kereš, D., Katz, N., Weinberg, D. H., & Davé, R. 2005, *MNRAS*, 363, 2
- Kewley, L. J. & Ellison, S. L. 2008, *ApJ*, 681, 1183
- Kitzbichler, M. G. & White, S. D. M. 2007, *MNRAS*, 376, 2
- Komatsu, E., Smith, K. M., Dunkley, J., et al. 2011, *ApJS*, 192, 18
- Kong, X. et al. 2006, *ApJ*, 638, 72
- Kornei, K. A., Shapley, A. E., Martin, C. L., et al. 2012, *ApJ*, 758, 135
- Krumholz, M. & Burkert, A. 2010, *ApJ*, 724, 895
- Kurk, J., Cimatti, A., Daddi, E., et al. 2013, *A&A*, 549, 63
- Kurk, J., Cimatti, A., Zamorani, G., et al. 2009, *A&A*, 504, 331
- Law, D. R., Steidel, C. C., Erb, D. K., et al. 2007, *ApJ*, 669, 929
- 2009, *ApJ*, 697, 2057
- Law, D. R., Steidel, C. C., Shapley, A. E., et al. 2012a, *ApJ*, 745, 85
- 2012b, *ApJ*, 759, 29
- Law, D. R., Shapley, A. E., Steidel, C. C. et al. 2012c, *Nature*, 487, 338
- Lemoine-Busserolle, M. & Lamareille, F. 2010, *MNRAS*, 402, 2291
- Lilly, S. J. et al. 2007, *ApJS*, 172, 70
- López-Sanjuan, C., Le Fèvre, O., Tasca, L. A. M., et al. 2012, *arXiv:1208.5020*
- Maiolino, R. et al. 2008, *A&A*, 488, 463
- Mancini, C., Foerster Schreiber, N., Renzini, A., et al. 2011, *ApJ*, 743, 86
- Mannucci, F. et al. 2009, *MNRAS*, 398, 1915
- Martin, C. L. 2005, *ApJ*, 621, 227
- Mas-Hesse, J. M. & Kunth, D. 1999, *A&A*, 349, 765
- Mayya, Y. D., Bressan, A., Rodríguez, M., Valdes, J. R., & Chavez, M. 2004, *ApJ*, 600, 188
- Mo, H. J., Mao, S., & White, S. D. M. 1998, *MNRAS*, 295, 319
- Murray, N., Quataert, E., & Thompson, T. A. 2005, *ApJ*, 618, 569
- Neichel, B., Hammer, F., Puech, M., et al. 2008, *A&A*, 484, 159
- Nelson, E. J., van Dokkum, P. G., Brammer, G., et al. 2012, *ApJ*, 747, L28
- 2012, submitted to *ApJ*
- Newman, S. F., Genzel, R., Förster-Schreiber, N., et al. 2012b, *ApJ*, 761, 43
- Newman, S. F., Shapiro Griffin, K., Genzel, R., et al. 2012a, *ApJ*, 752, 111
- Noeske, K. G. et al. 2007, *ApJ*, 660, L43
- Noguchi, M. 1999, *ApJ*, 514, 77
- Ocvirk, P., Pichon, C., & Teyssier, R. 2008, *MNRAS*, 390, 1326
- Oppenheimer, B. D. & Davé, R. 2006, *MNRAS*, 373, 1265
- 2008, *MNRAS*, 387, 577
- Oser, L., Ostriker, J. P., Naab, T., Johansson, P. H., & Burkert, A. 2010, *ApJ*, 725, 2312
- Ostriker, E. C. & Shetty, R. 2011, *ApJ*, 731, 41
- Peng, C. Y., Ho, L. C., Impey, C. D., & Rix, H.-W. 2002, *AJ*, 124, 266
- Peng, Y.-j., Lilly, S. J., Kovač, K., et al. 2010, *ApJ*, 721, 193
- Pettini, M. & Pagel, B. E. J. 2004, *MNRAS*, 348, L59
- Pettini, M., Steidel, C. C., Adelberger, K. L., Dickinson, M., & Giavalisco, M. 2000, *ApJ*, 528, 96
- Puech, M., Hammer, F., Flores, H., Neichel, B., & Yang, Y. 2009, *A&A*, 493, 899
- Puech, M., Hammer, F., Lehnert, M. D., & Flores, H. 2007, *A&A*, 466, 83
- Queyrel, J., Contini, T., Kissler-Patig, M., et al. 2012, *A&A*, 539, 93
- Rodighiero, G., Daddi, E., Baronchelli, I., et al. 2011, *ApJ*, 739, L40+
- Saintonge, A., Tacconi, L. J., Fabello, S., et al. 2012, *ApJ*, 758, 73
- Schreiber, J., Thatte, N., Eisenhauer, F., et al. 2004, in *ASP Conf. Ser. 314, Astronomical Data Analysis Software and Systems (ADASS) XIII*, ed. F. Ochsenbein, M. G. Allen, & D. Egret, 380
- Shapiro, K. L. et al. 2008, *ApJ*, 682, 231
- 2009, *ApJ*, 701, 955
- Shapley, A. E., Steidel, C. C., Pettini, M., & Adelberger, K. L. 2003, *ApJ*, 588, 65
- Steidel, C. C., Erb, D. K., Shapley, A. E., et al. 2010, *ApJ*, 717, 289
- Steidel, C. C., Shapley, A. E., Pettini, M., et al. 2004, *ApJ*, 604, 534
- Swinbank, A. M., Papadopoulos, P. P., Cox, P., et al. 2011, *ApJ*, 742, 11
- Swinbank, A. M., Sobral, D., Smail, I., et al. 2012a, *MNRAS*, 426, 935
- Swinbank, M., Smail, I., Sobral, D., et al. 2012b, *ApJ*, 760, 130
- Tacconi, L. J. et al. 2006, *ApJ*, 640, 228
- 2008, *ApJ*, 680, 246
- 2010, *Nature*, 463, 781
- 2012, *arXiv:1211.5743*
- Tremonti, C. A. et al. 2004, *ApJ*, 613, 898
- van den Bergh, S., Abraham, R. G., Ellis, R. S., et al. 1996, *AJ*, 112, 359
- van der Kruit, P. C. & Allen, R. J. 1978, *ARA&A*, 16, 103
- van Starckenburg, L., van der Werf, P. P., Franx, M., et al. 2008, *A&A*, 488, 99
- Veilleux, S., Cecil, G., & Bland-Hawthorn, J. 2005, *ARA&A*, 43, 769
- Veilleux, S., Cecil, G., Bland-Hawthorn, J., et al. 1994, *ApJ*, 433, 48
- Vergani, D., Epinat, B., Contini, T., et al. 2012, *A&A*, 546, 118
- Weiner, B. J., Willmer, C. N. A., Faber, S. M., et al. 2006, *ApJ*, 653, 1027
- Weiner, B. J. et al. 2009, *ApJ*, 692, 187
- Westmoquette, M. S., Smith, L. J., Gallagher, J. S., & Exter, K. M. 2007, *MNRAS*, 381, 913
- Wisnioski, E., Glazebrook, K., Blake, C., et al. 2012, *MNRAS*, 422, 3339
- Wisnioski, E., Glazebrook, K., Blake, C., et al. 2011, *MNRAS*, 417, 2601
- Wright, S. A., Larkin, J. E., Law, D. R., et al. 2009, *ApJ*, 699, 421
- Wright, S. A. et al. 2007, *ApJ*, 658, 78
- Wuyts, S., Förster Schreiber, N. M., Genzel, R., et al. 2012, *ApJ*, 753, 114
- Wuyts, S., Förster Schreiber, N. M., Lutz, D., et al. 2011, *ApJ*, 738, 106